

Multi-step-ahead Prediction from Short-term Data by Delay-embedding-based Forecast Machine

Hao Peng¹, Pei Chen^{1*}, Rui Liu^{1*}

¹ School of Mathematics, South China University of Technology, Guangzhou 510640, China.

* Correspondence should be addressed to PC: chenpei@scut.edu.cn; RL: scliurui@scut.edu.cn

Abstract

Making accurate multi-step-ahead prediction for a complex system is a challenge for many practical applications, especially when only short-term time-series data are available. In this work, we proposed a novel framework, Delay-Embedding-based Forecast Machine (DEFM), to predict the future values of a target variable in an accurate and multi-step-ahead manner based on the high-dimensional short-term measurements. With a three-module spatiotemporal architecture, DEFM leverages deep learning to effectively extract both the spatially and sequentially associated information from the short-term dynamics even with time-varying parameters or additive noise. Being trained through a self-supervised scheme, DEFM well fits a nonlinear transformation that maps from the observed high-dimensional information to the delay embeddings of a target variable, thus predicting the future information. The effectiveness and accuracy of DEFM is demonstrated by applications on both representative models and six real-world datasets. The comparison with four traditional prediction methods exhibits the superiority and robustness of DEFM.

Key word: Multi-step-ahead prediction; short-term time series; high-dimensional system; delay embedding; self-supervised learning.

Introduction

In the era of big data, various types of time-series data are widely observed in different fields, including the gene expression data of molecular biology, neural activity data of neuroscience, and atmospheric data of meteorology¹⁻⁷. In these areas, the availability of accurate empirical models for multi-step-ahead prediction is highly desirable. However, in view of the complexity and the nonlinearity of real-world systems, it is a challenging task to bridge from the known information to future dynamics, especially when the known time series contains only short-term time points and massive variables/factors. Recently, a number of approaches have been developed for time series analysis, e.g., statistical regression methods such as mean average through exponential smoothing^{8,9} and autoregressive integrated moving average model (ARIMA)¹⁰, the machine learning methods including methods^{11, 12} based on recurrent neural network (RNN)¹³, long-short-term-memory network (LSTM)¹⁴, lazy learning¹⁵, deep belief network¹⁶, and reservoir computing^{17, 18}. However, it is noted that most of both the statistical regression and machine

learning methods based on traditional neural network frameworks generally rely on long-term measurements of time series, which limits their applications to many real-world systems.

In contrast with a number of existing prediction methods based on long-term time series, few studies on multi-step-ahead predictions from short-term but high-dimensional data can be found. The short-term time series data are generally considered to have insufficient information for making prediction. Nevertheless, it is usually necessary to make predictions based on only a short-term series. On the one hand, because most real-world systems are time-varying and non-stationary, the short-term series that records the most recent temporal information captures the future dynamics more accurately than the long-term series that includes remote past information²³. On the other hand, for many practical scenarios such as biological experiment, only short-term series are available, which, however, possess rich information due to the high-dimensional observable biomolecules. Thus, new strategies are in demand to better explore the short-term time series observed from high-dimensional complex systems, whose dynamics are generally intertwined. Actually, the embedding theory¹⁹⁻²² reveals the fact that a high-dimensional attractor and reconstructed delay attractors with appropriately selected dimensions are topologically conjugated, thus suggesting mappings from the original attractor to the reconstructed ones. Recently, the randomly distributed embedding (RDE)^{23, 24} makes one-step-ahead prediction of a target variable based on short-term time series by transforming the high-dimensional information into the future evolution via the delay embedding theory. The challenging problem for this framework is how to solve the unknown nonlinear map between the sampled nondelay-attractors of high-dimensional variables and the delay-attractor of one target variable, where each attractor is numerically represented by a series of data points.

In this study, we propose a novel neural-network-based framework, delay-embedding-based forecast machine (DEFM), to make highly accurate multi-step-ahead prediction with short-term time-series data by transforming the spatial information of a high-dimensional dynamical system to the temporal information of a target variable (Fig. 1 (a)). Based on the delay embedding theory¹⁹⁻²², DEFM is designed to fit a nonlinear function that maps the observed high-dimensional variables to the delayed embeddings of a target/to-be-predict variable in a self-supervised manner. Specifically, instead of using a traditional neural network directly, DEFM utilizes its spatiotemporal structure consisting of a spatial and a temporal module to exploit the intrinsic dynamics of a complex system and extract both the spatial interactions and temporally associated information among variables from the high-dimensional data (Fig. 1(b)). With such data-driven architecture, DEFM takes high-dimensional variables as input neurons, and the delay embeddings of a target variable as the output neurons. Each high-dimensional vector (the input) paired with a delay-embedding vector of the target variable (the output) is taken as one training sample, which is equivalently regarded as an expansion of the training sample size and alleviates the overfitting problem due to the limited length of observed data. Therefore, DEFM is trained by a “consistently self-constrained scheme”, thus making multi-step-ahead prediction of a target variable in an accurate and robust manner even with only short-term data (Fig. 1 (b)). Besides, with the capability of obtaining multi-step-ahead future states in one prediction, DEFM can be applied to make the long-term prediction following an iterative scheme of taking the predicted values as a part of input for the next prediction.

To demonstrate the performance of DEFM, it has been applied to a ninety-dimensional coupled Lorenz system under different parametric and noise conditions, and a series of real-world systems, including the daily number of cardiovascular inpatients in major hospitals of Hongkong^{25, 26}, the wind speed and solar irradiance in Wakkanai, Japan²⁷, the route of typhoon center²⁸, the traffic speed of multiple nearby locations in Los Angeles²⁹, and the expression dynamics of genes related to circadian

rhythm³⁰. The results show that DEFM achieves multi-step-ahead prediction with only short-term time-series data, superior to other four existing methods in terms of both accuracy and robustness. Therefore, in consideration of the applicability in short-term series and reliable performance, DEFM offers a new way to make accurate multi-step-ahead prediction for complex systems and has great potential in practical application in many fields of artificial intelligence.

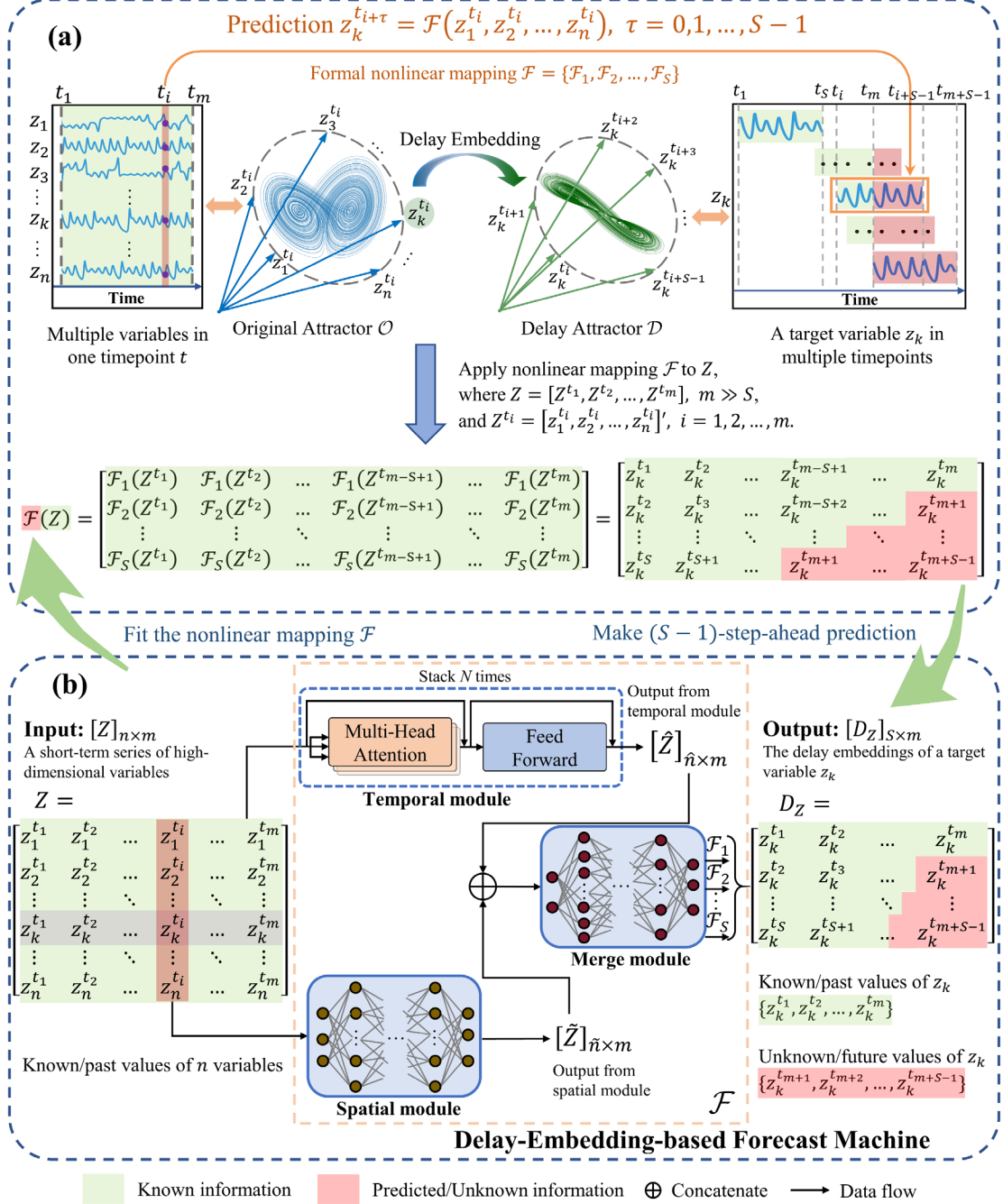


Fig. 1. The schematic illustration of the delay-embedding-based forecast machine (DEFM). (a) Through a delay embedding scheme²⁰⁻²², a delay attractor \mathcal{D} of a target variable z_k is reconstructed with appropriately reconstructed dimension, which is topologically conjugated to the original attractor \mathcal{O} . From attractor \mathcal{O} to \mathcal{D} , a formal nonlinear function \mathcal{F} maps the known spatial information into the temporal information of the target variable z_k , while the future values of z_k is obtained by $z_k^{t_i+\tau} = \mathcal{F}(z_1^{t_i}, z_2^{t_i}, \dots, z_n^{t_i})$, $\tau = 1, 2, \dots, S-1$. Therefore, the key of predicting z_k is to fit the nonlinear function \mathcal{F} . (b) For the given target

variable z_k , the DEFM framework is designed to fit the nonlinear mapping \mathcal{F} and thus offers a bridge between the high-dimensional data Z and the delay-embedding matrix D_z . DEFM fully extracts the rich spatial and temporal information from high-dimensional short-term data with a temporal and a spatial module, and integrates the spatiotemporal information via a merge module. After being trained in a self-supervised way, DEFM predicts the future information of z_k in a multi-step-ahead manner, i.e., simultaneously providing the unknown values $\{z_k^{t_{m+1}}, z_k^{t_{m+2}}, \dots, z_k^{t_{m+S-1}}\}$ in the output delay-embedding matrix D_z .

Results

The framework of DEFM

With the rapid development of deep learning, neural networks are utilized to fit a large variety of functions. However, a precise approximation depends on a well-designed network architecture that meets the requirements of a specific mission. The delay embedding theory guarantees that, under certain conditions for a proper choice of delay embedding dimension, the attractor reconstructed by delay embeddings is diffeomorphic to the original attractor¹⁹⁻²². Therefore, there is a nonlinear function \mathcal{F} that transforms the observed high-dimensional spatial information into temporal information of a target variable if $S > 2b > 0$ where S is the delay embedding dimension and b is the box-counting dimension of the original attractor. The detailed description of delay embedding theory and nonlinear function \mathcal{F} is provided in Methods and Supplementary Section 1. In order to make accurate prediction, the framework of DEFM is developed to approximate the nonlinear function \mathcal{F} based on the short-term high-dimensional time series (Fig. 1 (a)). Specifically, for a target/to-be-predicted variable $z_k \in \{z_1, z_2, \dots, z_n\}$ of an n -dimensional system, given high-dimensional time series $\{z_j^{t_1}, z_j^{t_2}, \dots, z_j^{t_m}\}$ ($j = 1, 2, \dots, n$) observed at m time points, the formal transformation $\mathcal{F} = \{\mathcal{F}_1, \mathcal{F}_2, \dots, \mathcal{F}_S\}$ holds as follow

$$\mathcal{F}(Z) = \begin{bmatrix} \mathcal{F}_1(Z^{t_1}) & \mathcal{F}_1(Z^{t_2}) & \dots & \mathcal{F}_1(Z^{t_m}) \\ \mathcal{F}_2(Z^{t_1}) & \mathcal{F}_2(Z^{t_2}) & \dots & \mathcal{F}_2(Z^{t_m}) \\ \vdots & \vdots & \ddots & \vdots \\ \mathcal{F}_S(Z^{t_1}) & \mathcal{F}_S(Z^{t_2}) & \dots & \mathcal{F}_S(Z^{t_m}) \end{bmatrix} = \begin{bmatrix} z_k^{t_1} & z_k^{t_2} & \dots & z_k^{t_m} \\ z_k^{t_2} & z_k^{t_3} & \dots & z_k^{t_{m+1}} \\ \vdots & \vdots & \ddots & \vdots \\ z_k^{t_S} & z_k^{t_{S+1}} & \dots & z_k^{t_{m+(S-1)}} \end{bmatrix} = D_z. \quad (1)$$

where $Z = [Z^{t_1}, Z^{t_2}, \dots, Z^{t_m}]_{n \times m}$ is the input matrix, $Z^{t_i} = [z_1^{t_i}, z_2^{t_i}, \dots, z_n^{t_i}]' \in \mathbb{R}^n$ is a vector containing n observed variables at time point $t = t_i$ ($i = 1, 2, \dots, m$), symbol “ ’ ” stands for the transpose of a vector. Delay-embedding matrix $[D_z]_{S \times m}$ is the output containing both known series $\{z_k^{t_1}, z_k^{t_2}, \dots, z_k^{t_m}\}$ and future series $\{z_k^{t_{m+1}}, z_k^{t_{m+2}}, \dots, z_k^{t_{m+S-1}}\}$ for the target variable z_k . Here, the target z_k can be any variable among $\{z_1, z_2, \dots, z_n\}$. To explore the intertwining information of observed short-term high-dimensional time series data, a spatiotemporal structure is deployed for the framework of DEFM, shown as in Fig. 1 (b). DEFM is composed of three modules, including a temporal, a spatial, and a merge module. The temporal module is assembled by a series of the so-called self-attention³¹ layers, which captures the underlying sequentially and temporally associated information among the input samples across all m observed time points. A spatial module for extracting the interactions among n variables from the high-dimensional data, and a merge module for processing the spatiotemporal information and outputting the transformed time series, are both implemented by two fully connected neural networks, respectively. Specifically, given matrix $Z \in \mathbb{R}^{n \times m}$, the collection of time-series data of high-dimensional variables $\{z_1, z_2, \dots, z_n\}$, as the input, there are two data-flow branches, i.e., each column $Z^{t_i} = [z_1^{t_i}, z_2^{t_i}, \dots, z_n^{t_i}]'$ of Z (a spatial vector at a time point $t = t_i$) is taken into the spatial module, while rows (the time series across all m time points $\{t_1, t_2, \dots, t_m\}$) are fed into

the temporal module. Then the outputs of temporal branch $\hat{Z} \in \mathbb{R}^{\hat{n} \times m}$ and that of spatial branch $\tilde{Z} \in \mathbb{R}^{\hat{n} \times m}$ are aggregated as one feature matrix through a concatenation operation, and input into the merge module. The detailed description of the three modules is presented in Methods.

Based on the DEFM architecture and the training samples paired with $[z_1^{t_i}, z_2^{t_i}, \dots, z_n^{t_i}]'$ and $[z_k^{t_i}, z_k^{t_{i+1}}, \dots, z_k^{t_{i+S-1}}]'$ with $i = 1, 2, \dots, m$, \mathcal{F} is fitted by a “consistently self-constrained scheme”. Specifically, due to the delay-embedding nature in the output D_z (as shown in equation (2)), we have the temporally self-constrained conditions

$$\mathcal{F}_{j-1}(Z^{t_{i+1}}) = \mathcal{F}_j(Z^{t_i}), \quad (2)$$

where $j \in \{2, 3, \dots, S\}$ and $Z^{t_i} = [z_1^{t_i}, z_2^{t_i}, \dots, z_n^{t_i}]'$ is a spatial sample at time point $t = t_i$ ($i = 1, 2, \dots, m$). Clearly, these cross-sample conditions in equation (2) constrains the training in terms of the temporal sequential of samples. Through an auto perception procedure, the training and optimization of DEFM is accomplished through a process of minimizing a loss function $\mathcal{L} = \mathcal{L}_{DS} + \mathcal{L}_{FC}$, where \mathcal{L}_{DS} is a determined-state loss quantifying the difference between the estimations and observed values based on the known states $\{z_k^{t_1}, z_k^{t_2}, \dots, z_k^{t_m}\}$ of z_k , and \mathcal{L}_{FC} is a future-consistency loss generated from the above self-constrained conditions (equation (2)) for the future/unknown series $\{z_k^{t_{m+1}}, z_k^{t_{m+2}}, \dots, z_k^{t_{m+S-1}}\}$ of z_k (see Methods for detailed definition). Therefore, in a self-supervised manner, DEFM is trained to fit the nonlinear function \mathcal{F} , and thus obtaining the future values $\{z_k^{t_{m+1}}, z_k^{t_{m+2}}, \dots, z_k^{t_{m+S-1}}\}$ of the target variable z_k .

Prediction results on a representative Lorenz dataset.

To illustrate the mechanism and performance of the DEFM framework, we employ a 90-dimensional (90D) coupled Lorenz system³² as the first representative model to generate synthetic time-series data, thus demonstrating the superior accuracy and reliability of DEFM. The Lorenz system is formally expressed as

$$\dot{Z}(t) = L(Z(t); P), \quad (3)$$

where variables $Z(t) = (z_1^t, \dots, z_{90}^t)'$, $L(\cdot)$ is a 90D function set of Lorenz system, and vector P represents the time-invariant parameters. The exact expression of the 90D coupled Lorenz system equation (3) and detailed description are provided in Supplementary Section 2.1.

First, DEFM was applied to a noise-free system equation (3), to predict the future dynamics of three randomly selected target variables z_{k_1} , z_{k_2} and z_{k_3} , respectively. The prediction was carried out with settings dimension $n = 90$, length of known series $m = 45$, and length of prediction $S - 1 = 18$, that is, in one prediction, DEFM provides a future time-series of 18-steps-ahead data for the targets, from the input of 45 known samples (each with 90 values). From a three-dimensional perspective (Figs. 2 (a)-(c)), DEFM predicts the future trends (the red curves) for all the targets $\{z_{k_1}, z_{k_2}, z_{k_3}\}$. It is seen that DEFM achieves the multi-step-ahead prediction not only for the single-wing case, i.e., the known/observed and the unknown/to-be-predicted time series are distributed in the same wing of the attractor as in Fig. 2(c)), but also for the cross-wing cases, i.e., the known/observed and the unknown/to-be-predicted time series are distributed in two different wings of the attractor as in Figs. 2 (a) and (b). Figures. S1 (d)-(l) present the accurate predictions of single target variables for the three cases, i.e., (d)-(f) for z_{k_1} , (g)-(i) for z_{k_2} , and (j)-(l) for z_{k_3} . For all the predictions of targets $\{z_{k_1}, z_{k_2}, z_{k_3}\}$, the Pearson Correlation Coefficients

(PCCs) between the eighteen predicted points and real values are all above 0.999, while the Root Mean Square Errors (RMSEs) are all below 0.06, which shows the high prediction accuracy of DEFM in both the single-wing and the cross-wing cases. More prediction results and details of the synthetic Lorenz dataset are shown in Supplementary Section 2.3.1.

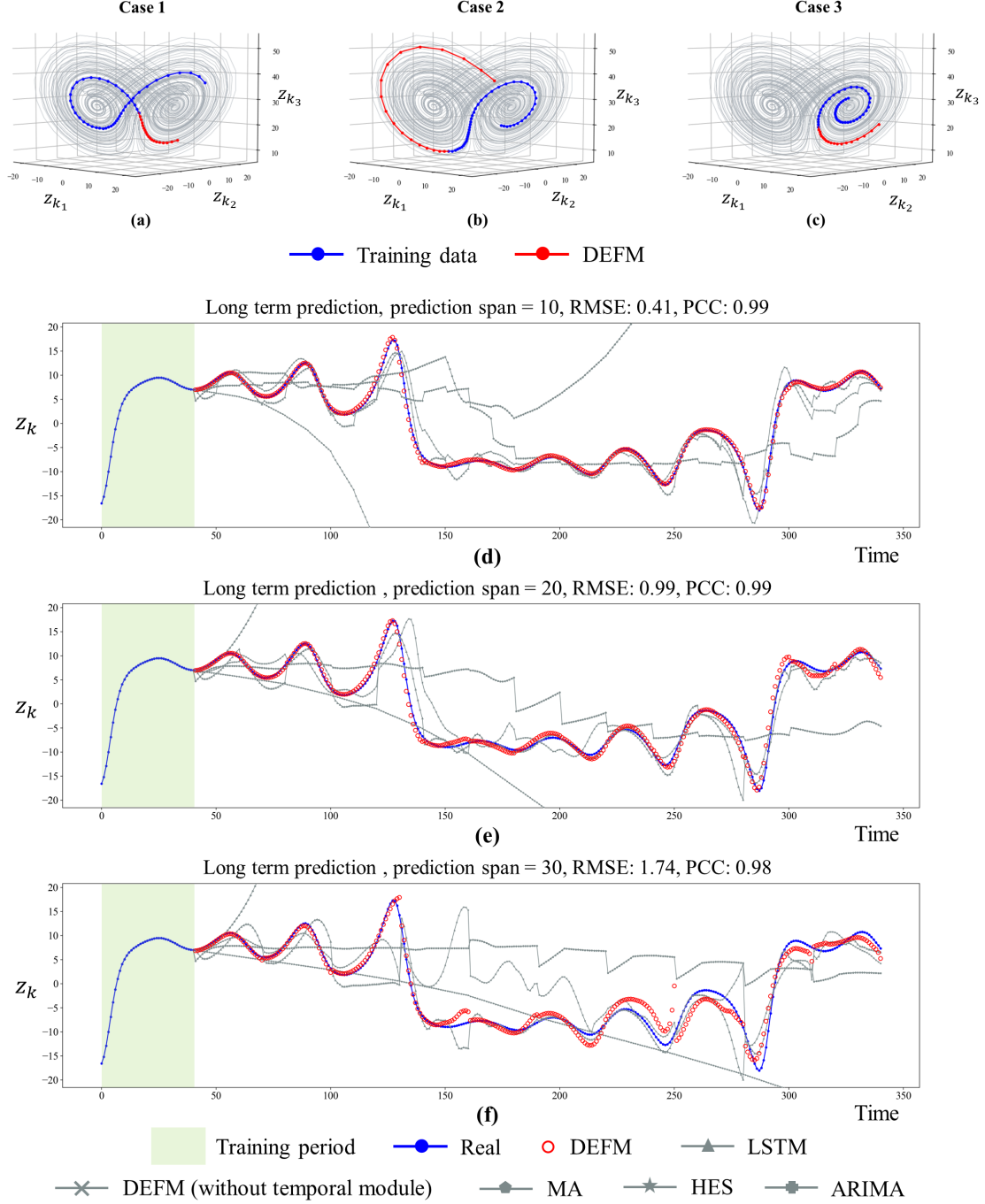


Fig. 2. The prediction performance of DEFM on a 90D synthetic Lorenz System equation (3). (a)-(c) The prediction results for three randomly selected target variables z_{k_1} , z_{k_2} and z_{k_3} in 3D systems. Long-term prediction results of DEFM on the Lorenz system with different predicting spans: (d): $S - 1 = 10$, (e): $S - 1 = 20$, (f): $S - 1 = 30$.

Long-term prediction

Owing to the capability of obtaining $(S - 1)$ -step-ahead future states in one prediction, DEFM can be applied to make the long-term prediction for an n -dimensional system with an iterative scheme.

Specifically, to forecast the long-term future states for a target variable z_k , say, $r(S - 1)$ -step-ahead future values ($r \geq 2$), DEFM is trained once (and remains fixed during the operation), and then applied for r times with the updated inputs. For each $(S - 1)$ -step-ahead prediction, the input matrix $[Z]_{n \times m}$ is updated by two parts of data: one part is the predicted series of a group of selected variables including the target, the other part is the observed time series of the remaining variables. As shown in Figs. 2 (d)-(f), DEFM was applied to the 90D coupled Lorenz system (equation (3)). It was trained by the initially observed data with length $m = 40$, and applied to make a long-term prediction (300 steps) with different predicting spans $(S - 1)$. It is seen that DEFM still forecast the long-term future values accurately when the span $S - 1 = 10$ (Fig. 2 (d)), while the predictions deviate from the real values when the span grows to $S - 1 = 20$ (Fig. 2 (e)) and $S - 1 = 30$ (Fig. 2 (f)).

Comparisons and robustness analysis

The spatiotemporal architecture of DEFM enables the full exploration of the temporally associated and spatially intertwined information from the observed time series of a high-dimensional system. To illustrate the superior performance of the proposed prediction method, the performance of DEFM is compared with other traditional prediction methods including the moving average (MA) which is the simplest method for time series forecasting by using the unweighted mean of previous values, Holt's Exponential Smoothing^{8, 9} (HES) which makes prediction by weighted moving average of previous values with exponentially changing weights, ARIMA¹⁰ which is a classical single-variable method and takes the trends, seasonality, cycles, errors and non-stationary aspects of temporal data into consideration, LSTM: Long short-term memory¹⁴ (LSTM) which is a famous method based on neural network for analysis of time series. Moreover, to illustrated the benefit brought by the temporal module, a simplified DEFM, which is of the same structure with DEFM except the temporal module is also applied in the comparison. The details of these five methods are listed in Supplementary Section 2.2.

First, DEFM and the other five prediction methods were applied to the dataset generated from the 90D coupled Lorenz system (equation (3)) with the length of unknown/to-be-predicted series in one prediction being fixed as 18, i.e., $S - 1 = 18$. Specifically, when the length of known time series $m = 80$, Fig. 3 (a) illustrates the prediction performances of all methods. It is seen that DEFM accurately predicts the unknown values of the target variable, better than the other methods (Table S1). As the known time series becomes shorter, DEFM still performs well with high accuracy when $m = 60$ (Fig. 3 (b)) and $m = 40$ (Fig. 3 (c)), better than the other methods (Table S1).

Second, the robustness of DEFM is shown in an application of the following 90D coupled time-varying Lorenz system

$$\dot{Z}(t) = L(Z(t); P(t)). \quad (4)$$

where $L(\cdot)$ is the same 90D nonlinear function set of the Lorenz system as in equation (3), but $P(t)$ is the time-varying/time-switching parameter vector, which alters when time variable t moves forward every 100 units. Notably, affected by external disturbance, most real-world systems are indeed time-varying rather than with constant parameters. Thus, the practical applicability of a prediction method should also be validated by the performance in such time-varying systems. As shown in Figs. 3 (d)-(f), when the length of known time series decreases, i.e., (d) $m = 80$, (e) $m = 60$, and (f) $m = 40$, DEFM performs stably and achieve the best accuracy among all methods in terms of both RMSE (all below 0.076) and PCC (all above 0.999). The training details of DEFM is presented in Supplementary Section

2.3.

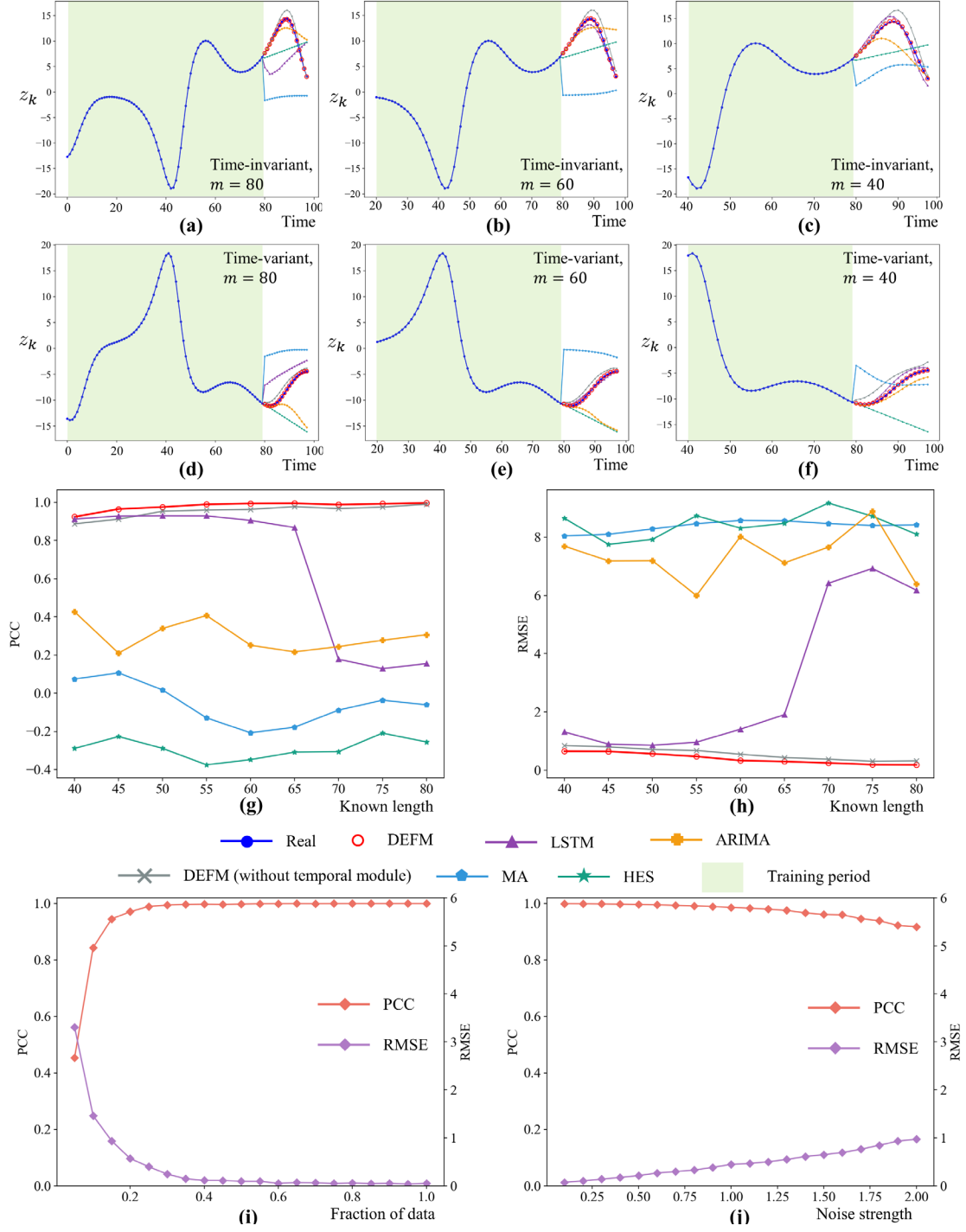


Fig. 3. Comparison results and robustness analysis results with the fixed length of predicted time series $S - 1 = 18$. Applying the six methods to the 90D coupled time-invariant Lorenz system (equation (3)), the prediction results with different settings of known length: (a) $m=80$, (b) $m=60$ and (c) $m=40$. The prediction results for the 90D coupled time-variant Lorenz system (equation (4)): (d) $m=80$, (e) $m=60$ and (f) $m=40$. For all 200 randomly chosen cases in the Lorenz system, (g) the average Pearson Correlation Coefficient (PCC) and (h) the mean root-mean-square error (RMSE) between predictions and real values as the length of known time series increases, changing from 40 to 80. (i) The average PCC and RMSE between predictions from DEFM and real values for cases with different data fractions. (j) The average PCC and RMSE between predictions from DEFM and ground truth for cases

with different noise strengths.

Moreover, for each value of the known length m ranging from 40 to 80, the comparison has been carried out in all cases of the high-dimensional Lorenz system. As shown in Figs. 3 (g) and (h), the DEFM method achieves the best prediction results with the highest PCC and lowest RMSE in terms of the average performance. Notably, even with short-term information observed from forty time points, DEFM still reaches mean PCC around 0.92 overall randomly selected cases, while the mean PCC and RMSE of other methods are much worse, demonstrating the excellent capability of DEFM in the short-term time-series analysis. Comparing with the stable performance of DEFM, it is also worth noting that, when the length of known series grows, the performance of LSTM becomes considerably poorer due to its limited memory³³.

To further validate the robustness of DEFM, the limited amount of training cases and noisy conditions were applied. With different fractions of all 1000 selected cases from the 90D coupled Lorenz system (equation (3)), DEFM was trained and tested. As shown in Fig. 3 (i), DEFM still works well after being trained by only 20% of selected cases, which suggests that the proposed framework can get rid of dependencies on a large amount of training data. Besides, noise is inevitable in real-world systems and disturbs data analysis. Trained by disturbed data generated from the 90D Lorenz system with white noise, DEFM was employed to predict the future values which were also been perturbed by the noise. Fig. 3 (j) shows that the performance of DEFM decreases gradually as the noise strength increases. However, even perturbed by considerably strong noise, i.e., the variation of noise is around 2.0, the average PCC and RMSE are acceptable.

From the above discussion, the robustness of DEFM is demonstrated by its superior performance in both time-invariant and time-varying systems with even short-term known series. In other words, the DEFM method is widely applicable for various high-dimensional systems and in different sampling conditions.

The application of DEFM on real-world datasets

In the era of big data, high-dimensional time series are observed and recorded in many real-world systems, which suggests the wide applicability of the DEFM method. In this study, DEFM shows its superior prediction performance in six high-dimensional real-world datasets, including the daily number of cardiovascular inpatients and recorded air pollutants, the wind speed and solar irradiance in a region, the route of typhoon center, the traffic situation of city transportation, and the biomolecular dynamics governed by circadian rhythm.

Air pollutants and hospital admission dataset. The air pollutants are recently considered as one of the causes of circulatory and respiratory diseases in big cities³⁴. In view of the high correlation between the cardiovascular inpatients and the air pollutants³⁵, DEFM was applied to predict the number of cardiovascular hospital admissions based on the air pollutant records. The cardiovascular inpatients dataset was gathered from 12 major hospitals in Hong Kong, while the severe air pollutants were recorded every day from 1994 to 1995 in the dataset^{25, 26}. For this application, the input is a 22-dimensional vector ($n = 22$) containing historical records of cardiovascular inpatients and common air pollutant indices such as concentrations of nitrogen dioxide (NO₂), sulphur dioxide (SO₂), ozone (O₃), respirable suspended particulate (Rsp_{ar}), etc. For each prediction based on DEFM, the known 22-dimensional time series with length $m = 100$ are used as the training data, and the prediction length is $S - 1 = 80$, i.e., the daily cardiovascular hospital admissions during a whole period of 80 future time points are to be

predicted. As illustrated in Fig. 4 (a), the predicting values by DEFM are highly coincident with the real data of hospital admission, with PCC up to 0.86 between the predicting and real data. Clearly, DEFM achieves the best accuracy among all prediction methods. For all cases, the average PCC 0.83 also shows the high accuracy and robustness of DEFM. More prediction results on the hospital admission dataset can be found in Supplementary Section 2.3.4.

Wind speed dataset. The wind speed is generally considered very difficult to predict. DEFM was employed to predict the instant wind speed for a whole period of future time points. The dataset of wind speed, provided by Japan Meteorological Agency²⁷, was collected at 155 meteorological stations every 10 minutes from January 2010 to December 2012 near the Wakkanai, Japan. In this application, the 155-dimensional time series is the input, i.e., $n = 155$, while the length of the known series is set as $m = 200$. For the target variable (the weed speed at a randomly selected site), the to-be-predicted length is set as 100, i.e., $S - 1 = 100$. As shown as in Fig. 4 (b), DEFM accurately forecasts the weed speed with high correlation coefficient $PCC=0.96$, showing a better performance than other prediction methods. For a set of 300 randomly chosen cases with the same settings, the average PCC between the predicted weed speed via DEFM and the real data reaches 0.93, and the RMSE is 0.589, which indicates that DEFM is capable of forecasting the future dynamical trend of weed speed in an accurate and robust manner. More prediction results on wind speed dataset are demonstrated in Supplementary Section 2.3.3.

Solar irradiance dataset. The third application is on the solar irradiance dataset which is also provided by Japan Meteorological Agency²⁷ and includes the data of solar irradiance from 155 meteorological stations recorded every 10 minutes from years 2010 to 2012, near Wakkanai, Japan. The settings are $n = 155$, $m = 150$ and $S - 1 = 50$, that is, the 155-dimensional records from 150 known time points are taken as the training data, while the solar irradiance at the subsequent 50 time points are to be predicted. In Fig. 4 (c), it is seen that the DEFM method predicts the future dynamics of solar irradiance for a randomly selected target meteorological station with PCC up to 0.99, better than other prediction methods. The average PCC between the predicted and the real dynamical trends reaches 0.965 for a set of 300 randomly chosen cases. More results can be found in Supplementary Section 2.3.5.

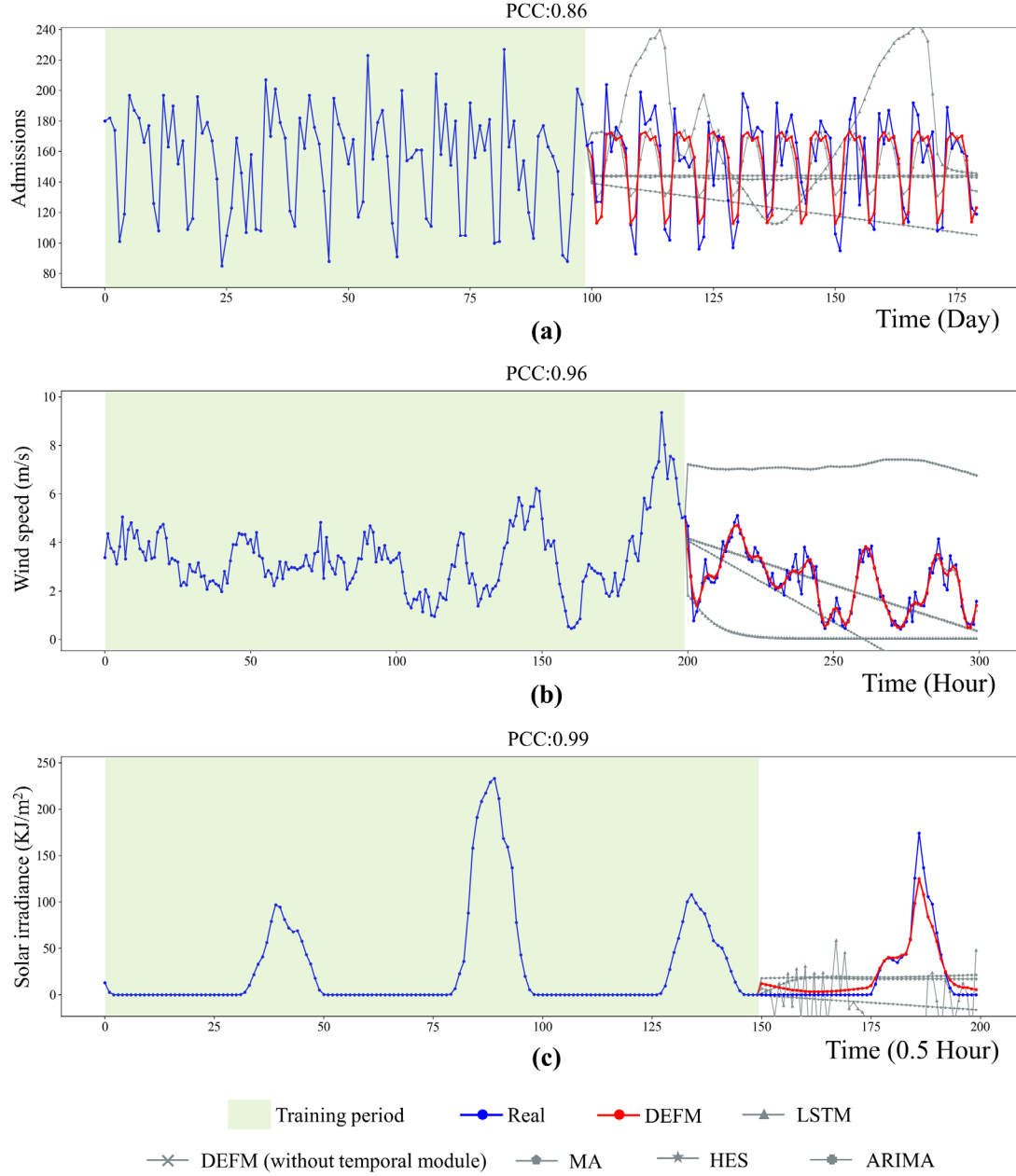


Fig. 4. The application of DEFM on hospital admission, wind speed, and solar irradiance datasets. (a) The 80-step-ahead prediction on cardiovascular disease admissions with $n = 22$, $m = 100$, and $S - 1 = 80$. DEFM prediction reaches PCC=0.86. (b) The 100-step-ahead prediction on wind speed dataset with $n = 155$, $m = 200$, and $S - 1 = 100$. DEFM prediction reaches PCC=0.96. (c) The 50-step-ahead prediction on solar irradiance with $n = 155$, $m = 150$, and $S - 1 = 50$. DEFM prediction reaches PCC=0.99.

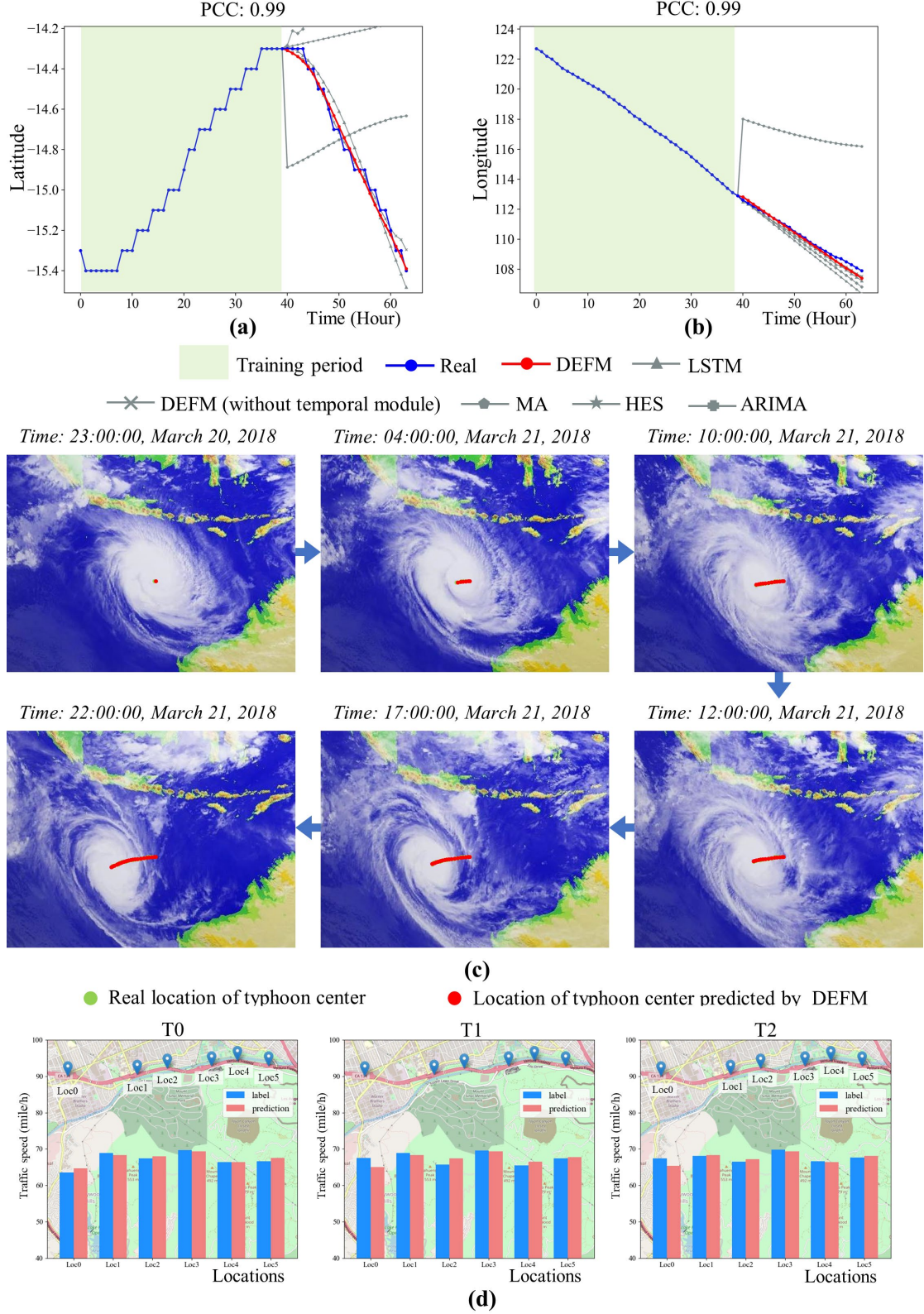


Fig. 5. Results of the predicted route of typhoon center and DEFM prediction results of multi-step prediction on traffic dataset. (a) The predicted dynamics of latitude of typhoon center. (b) The predicted dynamics of longitude of typhoon center. (c) Predicting route of typhoon Marcus in the next 24 hours from 23:00:00 20 March 2018 to 22:00:00 21 March 2018. (d) Predicted and real traffic speeds at 6 different neighboring locations for three adjacent time points.

Satellite cloud image dataset. An accurate prediction of the typhoon route is of crucial importance in disaster prevention, mitigation and response. As for the fourth application on real-world dataset, DEFM is employed to forecast the future position of the typhoon eye, based on 239 consecutive satellite cloud images of typhoon Marcus recorded per hour from 3/15/2018 to 3/24/2018. All original images are available in National Institute of Informatics²⁸. For each cloud image, one can extract the latitude and longitude of typhoon eye and 1200 pixels, while each pixel has two grayscale values. Therefore, there are totally $n = 2402$ variables at each time point. We select two variables, i.e., the latitude and longitude of typhoon eye, as the to-be-predicted targets. By setting $m = 40$ and $S - 1 = 24$, that is, using the images from past 40 hours as the known information or training series and predict the position of the Marcus' center for a period of upcoming 24 hours. As shown in Figs. 5 (a) and (b), the predicted latitude and longitude of typhoon eye reveals the dynamical trajectory of Marcus, which highly agrees to the ground truth. In Fig. 5 (c), it shows the predicted route of typhoon eye in the satellite cloud images starting from 23:00:00 3/20/2018 to 22:00:00 3/21/2018. The complete view of the route of Marcus from 3/20/2018 to 3/21/2018 is presented in Supplementary Section 2.3.6. A movie that shows the dynamical moving route of typhoon Marcus is provided in Supplementary Information Movie 1 (<https://github.com/Peng154/Delay-Embedding-based-Forecast-Machine>), which demonstrates the accurate prediction of the dynamical trajectory of the typhoon center.

Traffic dataset. This traffic dataset is composed of series data of traffic speed from 207 loop detectors in the highway of Los Angeles²⁹, which means that the dataset is an $n = 207$ -dimensional system. The interval of the data is five minutes. Considering these 207 loop detectors located on interconnected cities of the highway network, the traffic speed at all locations are interacting with each other. In this work, six nearby locations are randomly selected as the target variables. The time-series of $m = 50$ time points are used as the training data and the future values of the next $S - 1 = 10$ time points for the target detector are predicted. The prediction results are shown in Fig. 5 (d), which demonstrates that DEFM achieves an excellent performance towards all target variables. The prediction results for the other seven time-points results are shown in Supplementary Section 2.3.7. Also, a movie that shows the dynamical changes of the predicted and real traffic speeds in these six locations is given at <https://github.com/Peng154/Delay-Embedding-based-Forecast-Machine>.

Gene expression dataset. The last dataset is a gene expression data³⁰, which was measured on laboratory rats and utilized to study circadian rhythm. For this gene dataset, the expression of 31,099 genes were recorded for 22 time points, which infers a high-dimensional dynamical system with $n = 31099$ ³⁶. DEFM is applied to this gene dataset with $m = 12$ training time points and $S - 1 = 6$ prediction time points. Among all genes, eight were chosen as the to-be-predicted targets, including Nr1d2, Dbp, Cry1, Kif3c, Bmal1 (Arntl), Dec1 (Bhlhb2), Mapk6 and RGD1306883, which are known as genes related to circadian rhythm, a fundamentally important physiological process regarded as the "central clock" of mammals. As illustrated in Fig. 6, DEFM accurately predict the future trend of gene expressions not only for the key circadian genes such as Nr1d2, Dbp, and Cry1 which directly involve in circadian regulation of gene expression or entrainment of circadian clock by photoperiod, but also for the genes indirectly related to circadian rhythm such as Kif3c and RGD1306883. Clearly, among all six prediction methods, DEFM achieves the best accuracy, with PCCs all above 0.80, which demonstrates that DEFM has the potential applicability in functional analysis³⁷ by predicting the expressions of key genes.

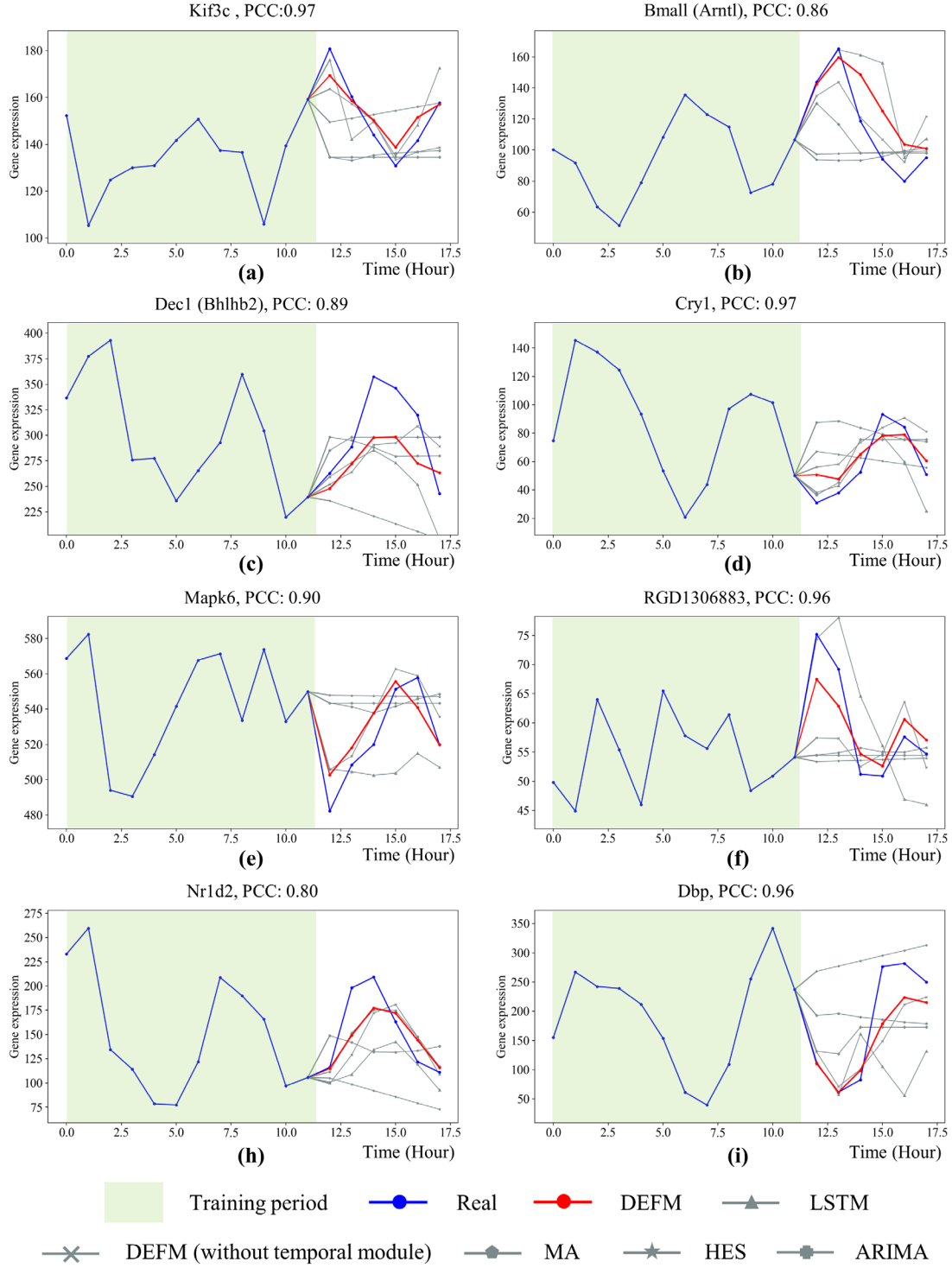


Fig. 6. The prediction results of gene expression of rats. Based on the DEFM framework, the dynamical trends of gene expressions in rats were accurately predicted for six circadian rhythm-related genes, i.e., Nr1d2, Dbp, Cry1, Kif3c, Arntl, and RGD1306883. In each prediction, the inputs included the expressions from the initial $m = 12$ time points, and the outputs of a multi-step-ahead prediction were the expressions for $S - 1 = 6$ time points ahead.

Conclusion

In this paper, we presented a novel dynamics-based machine learning model, i.e., DEFM, to make multi-

step-ahead prediction of the future information based on short-term time-series data. The key of the DEFM method is to approximate a nonlinear function that maps from the past/known information (the high-dimensional short-term time series of a complex system) to the future/unknown information (the time series of a target variable). Based on the delay-embedding scheme which enlarges the training sample size by including labeled embeddings and unlabeled future values (Fig. 1), DEFM makes use of high-dimensional short-term time-series data with its three spatiotemporal modules. Trained in a self-supervised way, DEFM well fits the nonlinear function and accurately predicts the future dynamics of the target variable in multi-step-ahead manner. Moreover, owing to the capability of obtaining multi-step-ahead future states in one prediction, DEFM can be applied to make the long-term prediction with an iterative scheme. From a series of applications, it is seen that DEFM accurately predict the future values of the target variable in both representative models and real-world datasets, which demonstrates its applicability in periodic-like datasets such as single-wing cases of Lorenz system (Case 3 in Fig. 2) and solar irradiance (Fig. 4 (c)), nonperiodic datasets such as two-wing cases of Lorenz system (Cases 1 and 2 in Fig. 2) and typhoon position (Fig. 5), and even in highly fluctuated cases such as wind speed (Fig. 4 (b)) and traffic flow (Fig. 5 (d)).

There are obvious advantages of the DEFM method. On the one hand, the well-designed architecture of DEFM composed of a temporal, a spatial, and a merge module makes it capable of fully exploring both the spatial interactions and temporally associated information among high-dimensional variables. On the other hand, comparing with the traditional prediction methods, DEFM performs more accurately and robustly with short-term time-series data from time-varying and noisy systems (Fig. 3), which is prevalent in practical applications. In view of these benefits, DEFM opens a new way to multi-step-ahead prediction with short-term time-series data, and is thus potentially useful in a wide variety of real-world systems.

Data availability

All data needed to evaluate the conclusions are present in the paper and/or the Supplementary Materials. All codes are available at github.com/Peng154/Delay-Embedding-based-Forecast-Machine.

Abbreviations

DEFM: Delay Embedding Forecast Machine.

ARIMA: AutoRegressive Integrated Moving Average model.

RNN: Recurrent Neural Network.

LSTM: Long-Short-Term-Memory network.

RDE: Randomly Distributed Embedding.

PCC: Pearson Correlation Coefficients.

RMSE: Root Mean Square Errors.

HES: Holt's Exponential Smoothing.

ALM: Anticipated Learning Machine.

Acknowledgement

This work was supported by National Natural Science Foundation of China (Nos. 11771152, 11901203,

11971176), Guangdong Basic and Applied Basic Research Foundation (2019B151502062), China Postdoctoral Science Foundation funded project (No. 2019M662895) and the Fundamental Research Funds for the Central Universities (2019MS111).

Author Contributions

Rui Liu, Pei Chen, and Hao Peng conceived the original idea and took the main writing work. Pei Chen collected the data. Hao Peng made main contribution to implementation of the DEFM framework and conducted the experiments along with Pei Chen and Rui Liu.

Disclosure of potential Conflict of Interests

The authors declare that they have no conflict of interest.

Additional Information

Supplementary Information includes Supplementary Text, Figs. S1-S8, Table S1.

References

- 1 Lockhart, D. J., & Winzeler, E. A. (2000). Genomics, gene expression and DNA arrays. *Nature*, 405(6788), 827.
- 2 Rienecker, M. M., Suarez, M. J., Gelaro, R., Todling, R., Bacmeister, J., Liu, E., ... & Bloom, S. (2011). MERRA: NASA's modern-era retrospective analysis for research and applications. *Journal of climate*, 24(14), 3624-3648.
- 3 Fan, J., Han, F., & Liu, H. (2014). Challenges of big data analysis. *National science review*, 1(2), 293-314.
- 4 De Jong, H. (2002). Modeling and simulation of genetic regulatory systems: a literature review. *Journal of computational biology*, 9(1), 67-103.
- 5 Stein, R. R., Bucci, V., Toussaint, N. C., Buffie, C. G., Ratsch, G., Pamer, E. G., ... & Xavier, J. B. (2013). Ecological modeling from time-series inference: insight into dynamics and stability of intestinal microbiota. *PLoS computational biology*, 9(12), e1003388.
- 6 Stevenson, I. H., & Kording, K. P. (2011). How advances in neural recording affect data analysis. *Nature neuroscience*, 14(2), 139.
- 7 Cohen, M. X. (2014). *Analyzing neural time series data: theory and practice*. MIT press.
- 8 Holt, C. C. (2004). Forecasting seasonals and trends by exponentially weighted moving averages. *International journal of forecasting*, 20(1), 5-10.
- 9 Brown, R. G. (1957, January). Exponential smoothing for predicting demand. In *Operations Research* (Vol. 5, No. 1, pp. 145-145). 901 ELKRIDGE LANDING RD, STE 400, LINTHICUM HTS, MD 21090-2909: INST OPERATIONS RESEARCH MANAGEMENT SCIENCES.
- 10 Box, G. E., & Pierce, D. A. (1970). Distribution of residual autocorrelations in autoregressive-integrated moving average time series models. *Journal of the American statistical Association*, 65(332), 1509-1526.

- 11 Parlos, A. G., Rais, O. T., & Atiya, A. F. (2000). Multi-step-ahead prediction using dynamic recurrent neural networks. *Neural networks*, 13(7), 765-786.
- 12 Giles, C. L., Lawrence, S., & Tsoi, A. C. (2001). Noisy time series prediction using recurrent neural networks and grammatical inference. *Machine learning*, 44(1-2), 161-183.
- 13 Connor, J. T., Martin, R. D., & Atlas, L. E. (1994). Recurrent neural networks and robust time series prediction. *IEEE transactions on neural networks*, 5(2), 240-254.
- 14 Hochreiter, S., & Schmidhuber, J. (1997). Long short-term memory. *Neural computation*, 9(8), 1735-1780.
- 15 Taieb, S. B., Sorjamaa, A., & Bontempi, G. (2010). Multiple-output modeling for multi-step-ahead time series forecasting. *Neurocomputing*, 73(10-12), 1950-1957.
- 16 Hinton, G. E., Osindero, S., & Teh, Y. W. (2006). A fast learning algorithm for deep belief nets. *Neural computation*, 18(7), 1527-1554.
- 17 Pathak, J., Hunt, B., Girvan, M., Lu, Z., & Ott, E. (2018). Model-free prediction of large spatiotemporally chaotic systems from data: A reservoir computing approach. *Physical review letters*, 120(2), 024102.
- 18 Maass, W., Natschl ger, T., & Markram, H. (2002). Real-time computing without stable states: A new framework for neural computation based on perturbations. *Neural computation*, 14(11), 2531-2560.
- 19 Sauer, T., Yorke, J. A., & Casdagli, M. (1991). Embedology. *Journal of statistical Physics*, 65(3-4), 579-616.
- 20 Takens, F. (1981). Detecting strange attractors in turbulence. In *Dynamical systems and turbulence, Warwick 1980* (pp. 366-381). Springer, Berlin, Heidelberg.
- 21 Packard, N. H., Crutchfield, J. P., Farmer, J. D., & Shaw, R. S. (1980). Geometry from a time series. *Physical review letters*, 45(9), 712.
- 22 Deyle, E. R., & Sugihara, G. (2011). Generalized theorems for nonlinear state space reconstruction. *PLoS One*, 6(3), e18295.
- 23 Ma, H., Leng, S., Aihara, K., Lin, W., & Chen, L. (2018). Randomly distributed embedding making short-term high-dimensional data predictable. *Proceedings of the National Academy of Sciences*, 115(43), E9994-E10002.
- 24 Ma, H., Zhou, T., Aihara, K., & Chen, L. (2014). Predicting time series from short-term high-dimensional data. *International Journal of Bifurcation and Chaos*, 24(12), 1430033.
- 25 Wong, T. W., Lau, T. S., Yu, T. S., Neller, A., Wong, S. L., Tam, W., & Pang, S. W. (1999). Air pollution and hospital admissions for respiratory and cardiovascular diseases in Hong Kong. *Occupational and environmental medicine*, 56(10), 679-683.
- 26 Fan, J., & Zhang, W. (1999). Statistical estimation in varying coefficient models. *The annals of Statistics*, 27(5), 1491-1518.
- 27 Hirata, Y., & Aihara, K. (2016). Predicting ramps by integrating different sorts of information. *The European Physical Journal Special Topics*, 225(3), 513-525.
- 28 Informatics, N. I. o. Digital Typhoon. <http://agora.ex.nii.ac.jp/digital-typhoon/summary/wsp/s/201820.html.en>
- 29 Li, Y., Yu, R., Shahabi, C., & Liu, Y. (2017). Diffusion convolutional recurrent neural network: Data-driven traffic forecasting. *arXiv preprint arXiv:1707.01926*.
- 30 Wang, Y., Zhang, X. S., & Chen, L. (2009). A network biology study on circadian rhythm by integrating various omics data. *OMICS A Journal of Integrative Biology*, 13(4), 313-324.

- 31 Vaswani, A., Shazeer, N., Parmar, N., Uszkoreit, J., Jones, L., Gomez, A. N., ... & Polosukhin, I. (2017). Attention is all you need. In *Advances in neural information processing systems* (pp. 5998-6008).
- 32 Curry, J. H. (1978). A generalized Lorenz system. *Communications in Mathematical Physics*, 60(3), 193-204.
- 33 Sutskever, I., Vinyals, O., & Le, Q. V. (2014). Sequence to sequence learning with neural networks. *Advances in NIPS*.
- 34 Metzger, K. B., Tolbert, P. E., Klein, M., Peel, J. L., Flanders, W. D., Todd, K., ... & Frumkin, H. (2004). Ambient air pollution and cardiovascular emergency department visits. *Epidemiology*, 46-56.
- 35 Xia, Y., & Härdle, W. (2006). Semi-parametric estimation of partially linear single-index models. *Journal of Multivariate Analysis*, 97(5), 1162-1184.
- 36 Shen-Orr, S. S., Milo, R., Mangan, S., & Alon, U. (2002). Network motifs in the transcriptional regulation network of *Escherichia coli*. *Nature genetics*, 31(1), 64.
- 37 Kang, S., Li, Q., Chen, Q., Zhou, Y., Park, S., Lee, G., ... & Alber, F. (2017). CancerLocator: non-invasive cancer diagnosis and tissue-of-origin prediction using methylation profiles of cell-free DNA. *Genome biology*, 18(1), 1-12.
- 38 Li, S., Jin, X., Xuan, Y., Zhou, X., Chen, W., Wang, Y. X., & Yan, X. (2019). Enhancing the locality and breaking the memory bottleneck of transformer on time series forecasting. In *Advances in Neural Information Processing Systems* (pp. 5244-5254).
- 39 Chen, Q., Zhao, H., Li, W., Huang, P., & Ou, W. (2019, August). Behavior sequence transformer for e-commerce recommendation in Alibaba. In *Proceedings of the 1st International Workshop on Deep Learning Practice for High-Dimensional Sparse Data* (pp. 1-4)
- 40 He, K., Zhang, X., Ren, S., & Sun, J. (2016). Deep residual learning for image recognition. In *Proceedings of the IEEE conference on computer vision and pattern recognition* (pp. 770-778).
- 41 Chen, C., Li, R., Shu, L., He, Z., Wang, J., Zhang, C., Ma, H., Aihara, K., Chen, L. (2020). Predicting Future Dynamics from Short-term Time Series by Anticipated Learning Machine. *National Science Review*. doi.org/10.1093/nsr/nwaa025